Phase tracking: an improved phase detection technique for cell membrane capacitance measurements

Nancy Fidler* and Julio M. Fernandez
Departments of Physiology and *Biophysics, School of Medicine, University of Pennsylvania, Philadelphia, Pennsylvania 19104-6085

ABSTRACT We describe here a technique called phase tracking that greatly improves the accuracy of measurements of the membrane capacitance of single cells. We have modified the original phase detection technique to include a method for creating calibrated changes in the resistance in series with the cell. This provides a method to automate the adjustment of the phase detector to the appropriate phase angle for measuring membrane capacitance. The phase determination depends only on the cell's electrical parameters and does not require matching of the cell impedance with that of the slow capacitance cancellation circuitry of the patch-clamp amplifier. We show here that phase tracking can accurately locate the phase of the capacitance signal and can keep the detector aligned with this signal during measurements of exocytosis in mast cells, irrespective of the large drifts which occur in cell membrane resistance, membrane capacitance, or series resistance. The phase tracking technique is a valuable tool for quantifying exocytosis and endocytosis in single cells.

INTRODUCTION

Measurement of the cell membrane capacitance is a useful assay to determine changes that occur in cell membrane area. This was first demonstrated by an experiment in which an increase in capacitance, measured in a suspension of sea urchin eggs, was observed to follow fertilization and exocytosis of cortical granules (Cole, 1935). Subsequently, intracellular recording allowed capacitance increases to be measured in single sea urchin eggs (Jaffe et al., 1978), and during exocytosis of synaptic vesicles in single isolated terminals of the squid giant synapse (Gillespie, 1979). However, the amplitude of individual exocytotic events underlying the macroscopic capacitance increases could not be resolved in these experiments. Then in 1982, Neher and Marty, utilizing the whole cell current recording mode of the patch-clamp technique and a phase sensitive detector, measured the small changes in the plasma membrane capacitance associated with single granule fusion and membrane retrieval events in isolated bovine adrenal chromaffin cells. With this development, the measurement of membrane capacitance has become an important technique for studying exocytosis, endocytosis, and stimulus-secretion coupling mechanisms in a variety of cells (Neher and Marty, 1982; Fernandez et al., 1984; Zimmerberg et al., 1987; Breckenridge and Almers, 1987*a*, *b*; Neher, 1988; Mason et al., 1989; Schweizer et al., 1989).

Address reprint requests and correspondence to Dr. Julio M. Fernandez, Department of Physiology and Biophysics, Mayo Foundation, Rochester, MN 55905.

The phase detection technique measures changes in a sinusoidal membrane current that occur at a specific phase angle, θ, with respect to a sinusoidal voltage stimulus and which are proportional to changes in membrane capacitance. The change in current at θ has to be calibrated in order to convert it into an equivalent change in capacitance. There are, however, several problems with the technique that limit the accuracy and range over which capacitance changes can be measured. The most severe of these is the fact that the impedance of a cell can change significantly during the course of a typical experiment. Since both θ and the calibration depend on the cell impedance, large changes occur in θ and in the calibration factor. Significant errors result if a stationary phase detector is used, and if the change in the calibration is not taken into account (Joshi and Fernandez, 1988). Therefore, to obtain accurate capacitance measurements, it has been necessary to interrupt the recording to determine a new θ and new calibration after significant impedance changes occur. This is time consuming and much of the capacitance data is lost.

This paper will describe a new technique, called phase tracking, that is able to find θ in real time throughout an experiment, and that eliminates the problem of the capacitance signal drifting out of phase with the detector. The technique can also track changes in the calibration scale that convert the current measured at θ into units of capacitance. We evaluated the performance of phase tracking using an equivalent circuit model of the cell impedance, and also by following large numbers of exocy-

0006-3495/89/12/1153/10 $2.00

totic events in degranulating mast cells. The use of phase tracking results in a dramatic increase in the reliability and amount of data obtained from single cells. A preliminary report of this work has appeared in abstract form (Fidler and Fernandez, 1989).

MATERIALS AND METHODS

Mast cell preparation and solutions

Peritoneal mast cells were obtained from 8-wk-old mice by peritoneal lavage. The collected cells were centrifuged, resuspended, and plated on glass coverslips in a solution containing (in millimolar) 136 NaCl, 9 Hepes, 2.5 KOH, 1.4 NaOH, 0.9 $MgCl_2$, 1.8 $CaCl_2$, 45 $NaHCO_3$, 6 glucose, and 0.4 K-phosphate buffer. The cells were incubated at 37°C and in 5% CO_2 for at least 30 min before use. For patch clamp experiments, the external solution was exchanged to (in millimolar) 150 NaCl, 10 Hepes, 2.8 KOH, 1.5 NaOH, 1 $MgCl_2$, 2 $CaCl_2$, and 25 glucose (310 mmol/kg, pH 7.2–7.3). The internal pipette solution contained (in millimolar) 140 K-glutamate, 10 Hepes, 7 $MgCl_2$, 3 KOH, 0.2 ATP, and 4 EGTA (290 mmol/kg, pH 7.2–7.3). We included 4 μM GTP-γS in the internal solution in these experiments to stimulate mast cell degranulation (Fernandez et al., 1984). Cell currents were recorded at room temperature.

Recording system

Cell membrane current was recorded with an EPC-7 patch-clamp amplifier using the whole cell mode of the patch-clamp technique (Hamill et al., 1981). The command potential of the amplifier was controlled by a PDP 11/73 computer and an INDEC Systems data acquisition interface. The stimulus voltage used for recording capacitance is a 60-mV, 833-Hz sine wave superimposed on a holding potential of about −10 mV. The output signal of the patch clamp amplifier was analyzed using a software-based phase detector (Joshi and Fernandez, 1988). The sampling interval of the detector outputs in the experiment of Fig. 4 was 38 ms. In a recent implementation of phase-tracking, using a Compaq 386/25 microcomputer equipped with a C Lab interface, we currently operate with a time resolution of 12 ms/point (Alvarez de Toledo, G., personal communication).

Phase detection theory

Consider Fig. 1 *A*, which shows an equivalent circuit representation of a patch-clamped cell and includes the contribution of the slow capacitance cancellation circuitry in the total current measured by the I-V converter. A sinusoidal voltage applied to the cell through the command input (V_{com}) will produce a sinusoidal current response which is phase shifted with respect to V_{com}. This current can be represented in complex space as a vector,

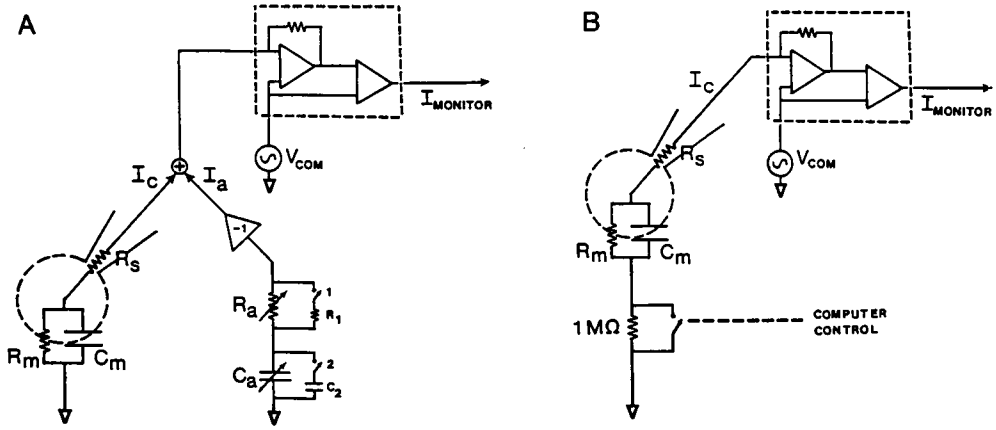

FIGURE 1 Schematic diagram of a patch-clamped cell for two different methods of recording membrane capacitance and locating θ. The I-V converter of the patch clamp amplifier (*boxed region*) measures current flowing in response to a voltage stimulus applied at the command input, V_{com}. (*A*) In the original method, current from the cell, I_c is added to the current from the transient cancellation circuitry of the amplifier, I_a, at the summing junction. The equivalent circuit model for a patch-clamped cell consists of a series resistance, R_s, and the cell membrane resistance, R_m, and capacitance, C_m. The right branch of the circuit represents (in principle only) the major elements of the capacity cancellation circuitry of the EPC-7, where R_a and C_a are variable resistance and capacitance settings. R_1 and C_2 (−100 fF) are elements in parallel with R_a and C_a, respectively. Switches 1 and 2 can be closed and opened to create controlled changes in the amplifier current due to a known amplifier resistance or capacitance change. (*B*) For the phase tracking technique, a 1-MΩ resistor is added in series with the cell. In parallel with the 1-MΩ resistor is a reed relay switch (model W171DIP; Magnecraft from Newark Electronics, Chicago, IL), the position of which is controlled by a 5-V coil voltage supplied by a digital to analog converter.

completely defined by two parameters: a magnitude, and a phase angle measured with respect to the real axis (or V_{com}, which is defined to have a phase = 0°). At this point, we need to briefly review the principles of the phase detection technique as derived by Neher and Marty, 1982, and Joshi and Fernandez, 1988. We need to rewrite the equations from these references in terms of the cell impedance, Z, because with phase tracking we create changes in series resistance.

For the simple three-element equivalent circuit of a patch clamped cell in Fig. 1, the current due to a sinusoidal voltage stimulus, will be given by $I = V/Z$, or

$$I = \frac{j\omega C_m + 1/R_m}{j\omega C_m R_s + R_s/R_m + 1} \cdot V, \quad (1)$$

where $V = V_{com}(\omega, t) = V \sin(\omega t)$ and $\omega = 2\pi f = 5234/s$. In what follows, we will make the assumption that $1/R_m \ll \omega C_m$ (see Discussion and Lindau and Fernandez, 1986). Given Eq. 1, there is no way to isolate a vector component of I that is directly proportional to the total capacitance. However, changes in any of the parameters, C_m, R_m, or R_s, will produce a change in the current through the cell membrane, ΔI. A phase-sensitive detector can be used to isolate a component of ΔI that is proportional to changes in capacitance only. The total change in current can be separated into the following components:

$$\Delta I = \Delta I_{R_m} + \Delta I_{C_m} + \Delta I_{R_s}, \quad (2)$$

where ΔI_{C_m}, ΔI_{R_m}, and ΔI_{R_s} are the changes that occur due to small changes in either C_m, R_m, or R_s, respectively. The relevant current components of ΔI are given by

$$\Delta I_{R_m} = \frac{\partial I}{\partial R_m} \Delta R_m = \frac{-1}{R_m^2} VB^2 \Delta R_m \quad (3)$$

$$\Delta I_{C_m} = \frac{\partial I}{\partial C_m} \Delta C_m = j\omega VB^2 \Delta C_m \quad (4)$$

and

$$\Delta I_{R_s} = \frac{\partial I}{\partial R_s} \Delta R_s = \omega^2 C_m^2 VB^2 \Delta R_s \quad (5)$$

where,

$$B^2 = \left(\frac{1}{1 + j\omega C_m R_s} \right)^2. \quad (6)$$

The argument of ΔI_{C_m}, θ, is given by

$$\theta = \pi - 2 \tan^{-1}(\omega C_m R_s). \quad (7)$$

The vector ΔI_{C_m} is the quantity of interest in measurements of membrane expansion because it is proportional to ΔC_m and orthogonal to ΔI_{R_s} and ΔI_{R_m} (caveat, see Neher and Marty, 1982 or Joshi and Fernandez, 1988).

Phase tracking

The most critical step in measuring cell membrane capacitance with the phase detection technique is to determine the phase angle, θ, of ΔI_{C_m}. When the phase detector is set at θ, current changes proportional to small capacitance changes can be measured with maximum resolution and without interference from currents produced by changes in the other electrical parameters of the cell. If θ is the phase of the capacitance signal, we will therefore use the term θ-90° to specify the phase of ΔI_{R_s}. The procedure introduced by Neher and Marty (and subsequently modified by Joshi and Fernandez) for finding θ requires matching of the cell impedance (strictly, only C_m and R_s) with the impedance of the slow capacity cancellation circuitry of the amplifier (C_a and R_a in Fig. 1 *A*). Then, a small change in R_a, created by temporarily closing switch 1, would allow the current component at θ-90° to be identified. The capacitance signal is located perpendicular to this component, at θ. A small known change in C_a equal to 100 fF, created by temporarily closing switch 2, would then provide a calibration for the capacitance signal measured at θ (see Joshi and Fernandez, 1988; Lindau and Neher, 1988). Note that the impedance of the cell and of the compensation circuitry must be exactly equal to guarantee that a small change in R_a is identical to a small change in R_s, and likewise for C_a and C_m. Although this procedure is effective, matching the impedances is often time consuming and error prone.

The phase tracking technique provides a faster, more direct way of finding θ-90°, and is illustrated in Fig. 1 *B*. We connected a 1-MΩ resistor in series with the cell, between the bath electrode and the ground return of the patch-clamp headstage. A computer-controlled reed relay switch connected in parallel with the 1-MΩ resistor can be transiently opened, causing an increase in R_s of exactly 1 MΩ. This calibrated change in R_s causes a proportional change in the current component at θ-90° only. Again, the capacitance signal can be located by moving the detector 90° away from the R_s changes. This procedure can find the real value of θ for any value of the cell's impedance. Furthermore, the phase tracking method is independent of the R_a or C_a settings, eliminating the requirement of matching the impedance of the cell to that of the cancellation circuitry. This technique is also applicable to cells whose impedance cannot be well matched by the single time constant equivalent circuit of the amplifier. Most importantly, phase tracking can be used throughout large increases in C_m, such as those observed during mast cell degranulation, to track the phase angle of the capacitance signal.

We will now describe in more detail how to calculate in real time the phase of ΔI_{R_s}, and thus also the phase of ΔI_{C_m}. The sinusoidal cell current is first measured with the relay switch closed. The phase detector, set 0° and 90° with respect to V_{com}, measures the projection of the total current (I in Eq. 1) on the real and imaginary axes. This measurement is repeated for the open position of the relay. The difference between the total current measured at each switch position is the change in current, ΔI_{R_s}, resulting from a 1-MΩ increase in R_s. The difference current at each phase detector output, ΔI_0 and ΔI_{90}, are therefore the projections of the vector ΔI_{R_s} at 0° and 90°. The magnitude and phase of ΔI_{R_s} can then be calculated from

$$|\Delta I_{R_s}| = \sqrt{\Delta I_0^2 + \Delta I_{90}^2}$$

$$\arg(\Delta I_{R_s}) = \theta - 90° = \tan^{-1}\left(\frac{\Delta I_{90}}{\Delta I_0}\right).$$

The argument of the vector ΔI_{R_s} is equal to the angle between the stimulus at 0° and ΔI_{R_s}, which we have called θ-90°. The output of the phase detector, which will measure capacitance, is then moved at right angles to the calculated phase of ΔI_{R_s}, i.e., to θ. The other detector output will therefore report changes in current at θ-90° due to changes in both R_s or R_m.

Two measurements are needed to specify ΔI_{R_s}, i.e., current with the relay switch closed and current with the relay switch open. After calculating θ, the phase detector is moved to θ to measure ΔI_{C_m}. If phase tracking were used continuously, each capacitance data point would consist of three current measurements with the phase detector. This would slow down our present time resolution by at least a factor of three, and is therefore undesirable. Instead, we choose to calculate θ only once every 256 points or about once every 10 s. This is a compromise which does not let ΔI_{C_m} drift too far from the detector, and at the same time does not reduce our average temporal resolution/point. This compromise also makes it possible to reduce the errors in each calculation of θ by averaging several pairs (relay open and closed) of current measurements to determine ΔI_{R_s}.

Calibrating the capacitance record

A proportionality factor must be determined in order to convert the change in current at θ into farads. At the beginning of an experiment, a calibration of the capacitance trace is obtained by means of the slow capacitance cancellation circuitry, as described before for Fig. 1 *A*. This calibration generates a transient change in C_a that is equivalent to a 100-fF change in C_m. However, the calibration will very rapidly become inaccurate as C_m, R_s, and R_m drift from the initial, compensated values during an experiment. This is because the proportionality factor between ΔI_{C_m} and ΔC_m is not constant, but depends on the cell impedance (Eq. 4). Significant errors result if it is assumed that an initial 100-fF calibration is accurate over the whole range of C_m recorded (see Joshi and Fernandez, 1988).

We will now describe how to estimate the change in the calibration, without having to interrupt the C_m recording, compensate the new capacity transient, and give a new calibration with the cancellation circuitry. It is still necessary to experimentally determine the initial calibration using the amplifier cancellation circuitry. Subsequent calibrations are obtained using this initial scale and the change in the calibration estimated with the phase tracking method. The method requires that phase tracking be used to always keep the detector aligned with the capacitance signal, and also uses the ability to make calibrated (e.g., 1 MΩ) changes in the R_s of the cell.

Suppose that $|\Delta I_{C_m}(0)|$ is the change in current due to a 100-fF change in capacitance used as the calibration at the start of a recording. The same 100-fF change in capacitance, if given at some time later, t, for a new cell impedance would cause a different change in current, $|\Delta I_{C_m}(t)|$. Because the detector is aligned with θ, we use the symbol, $|\ |$, to indicate that the output is the absolute magnitude of ΔI_{C_m}, not simply the real part of the complex quantity ΔI_{C_m}. The ratio of the calibrations, is defined as

$$CF = \frac{|\Delta I_{C_m}(0)|}{|\Delta I_{C_m}(t)|}. \tag{8}$$

In this expression, $|\Delta I_{C_m}(t)|$ is an unknown since we do not stop to find a new calibration after the cell impedance changes. If we can find an equivalent expression for CF, we could compute the size of the new calibration at time t. Alternatively, we could multiply capacitance changes at t by the factor CF, so that the current changes at 0 and t are equal in amplitude for an equal change in C_m at 0 and t. In other words, CF could be used as a data correction factor to eliminate the problem of a change in the calibration scale due to large cell impedance changes. Substituting expressions for ΔI_{C_m} from Eq. 4 into Eq. 8, with ω, V, and ΔC_m constant gives

$$CF = \frac{|B^2(0)|}{|B^2(t)|}. \tag{9}$$

This equation tells us that the variation in the current magnitude for a small constant capacitance change is due entirely to variations in the term $|B^2|$. This is because B^2 is the only term in the proportionality between ΔI_{C_m} and

ΔC_m which is not constant, but which depends on C_m and R_s.

We still do not know CF since we do not know $|B^2(t)|$ (we can determine $|B^2(0)|$ from the initial calibration). We do, however, have a knowledge of the proportionality between $|\Delta I_{R_s}|$ and ΔR_s, since phase tracking allows us to create a known change in the series resistance of the cell. We can then make use of Eq. 5 to find $|B^2|$. Since ΔR_s in this equation is constant, we find

$$\frac{|B^2(0)|}{|B^2(t)|} = \frac{C_m^2(t)}{C_m^2(0)} \cdot \frac{|\Delta I_{R_s}(0)|}{|\Delta I_{R_s}(t)|}, \tag{10}$$

where $|\Delta I_{R_s}|$ is the magnitude of the current change at θ-90° due to a 1-MΩ ΔR_s at 0 and t. If we can determine C_m at 0 and t, then we can find the factor by which $|B^2|$ is affected due to any intervening changes in C_m or R_s. Substituting Eq. 10 into 9 gives

$$CF = \frac{C_m^2(t)}{C_m^2(0)} \cdot \frac{|\Delta I_{R_s}(0)|}{|\Delta I_{R_s}(t)|}. \tag{11}$$

An example of the use of Eq. 11 is given in Results.

RESULTS

Experiments using an equivalent circuit model of a patch-clamped cell

Fig. 2, *A* and *B*, illustrates a problem associated with the original technique that we have addressed with phase

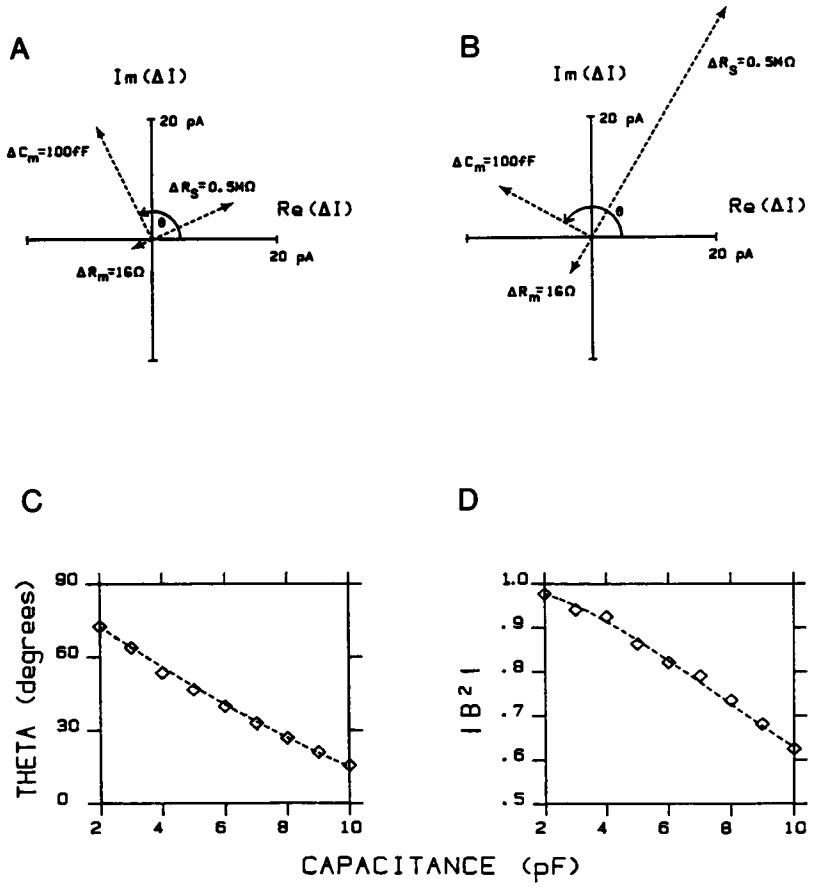

FIGURE 2 Both the phase angle for measuring capacitance and the calibration scale depend on input cell impedance. (*A* and *B*) Fixed changes in either C_m(100 fF), R_s(0.5 MΩ), or R_m(1 GΩ) produce current changes which are plotted as vectors in complex space. Current magnitudes and phases were calculated from Eqs. 3–5 using ω = 5,234/s and V = 40 mV. The vectors in *A* use C_m = 5 pF, R_s = 7 MΩ, and R_m = 10 GΩ. The vectors in *B* were calculated for a different cell impedance: C_m = 10 pF, R_s = 10 MΩ, and R_m = 5 GΩ. Theta (θ) is the phase angle of ΔI_{C_m} measured with respect to real axis. In both *A* and *B*, ΔI_{C_m} is exactly perpendicular to ΔI_{R_m}; however, we did not make the assumption here that $R_m \gg 1/\omega C_m$, and thus ΔI_{C_m} is not perpendicular to ΔI_{R_s}. The angle between the vectors ΔI_{Cm} and ΔI_{Rs} in both *A* and *B* was found to be 89.6°. Also, the calculated magnitude of ΔI_{R_m} is so small compared with ΔI_{R_s} or ΔI_{C_m}, that for clarity it is shown enlarged by a factor of five in both *A* and *B*. (*C* and *D*) The change in θ and $|B^2|$ is shown for the capacitance range 2–10 pF. The dashed curves are theoretical predictions of the change in θ and $|B^2|$ calculated from Eqs. 7 and 6, respectively, with R_s = 14.7 MΩ and ω = 5,234/s. ◇, experimental determinations of θ and $|B^2|$ using the phase tracking technique.

tracking. We show the effect of a change in cell impedance on the magnitude and location of the current vector, ΔI_{C_m}. In both *A* and *B*, current changes were calculated for ΔC_m = 100 fF, ΔR_s = 0.5 MΩ, and ΔR_m = 1 GΩ. The only difference between *A* and *B* is in the values of C_m, R_s, and R_m used for the calculation. In *A* the impedance was typical of a resting mast cell while the impedance used in *B* was typical of a partially degranulated mast cell. Note that in *B*, the phase angle, θ, of the current vector, ΔI_{C_m}, is shifted by 35° and the magnitude is reduced by ~20% as compared with *A*. The current vectors, ΔI_{R_s} and ΔI_{R_m}, also change in magnitude and phase, but remain perpendicular to ΔI_{C_m}.

To test the performance of phase tracking in finding θ and the fractional change in the calibration, we first used an RC series circuit, connected to the input of the amplifier headstage, to model the R_s and C_m of a real cell. Since the "cell" impedance is therefore known at all times, we compared calculated parameters with experimental results measured with phase tracking. In these experiments, we assumed that R_m was very large and could be ignored. We first adjusted the R_a and C_a of the amplifier to exactly compensate the capacity transient of the equivalent circuit. The best cancellation occurred when C_a = 2 pF and R_a = 14.7 MΩ, presumably the actual values in the RC circuit at the headstage. At this point, the R_a and C_a of the amplifier are exactly matched to the input RC series circuit. We then reversed the roles of the cancellation circuitry and the actual equivalent circuit, such that the former was used to simulate a real cell. This was done in order to facilitate changing the "cell" parameters, since this could be accomplished simply by changing the R_a or C_a dials of the patch-clamp amplifier. The exact equivalent of phase tracking was implemented using R1 and switch 1 in the cancellation circuitry (See Fig. 1 *A*).

Eq. 7 describes the dependence of θ on the cell parameters. The predicted change in θ from this equation over the C_m range 2–10 pF is plotted in Fig. 2 *C* (---------). We increased C_a by 1-pF increments, starting from 2 pF, and at each capacitance found the new phase angle as outlined in Methods. The results with the phase tracking technique (◊) exactly overlap the predicted θ over the whole range of capacitance. Thus we have demonstrated, for an RC series approximation of a real cell, that the phase tracking technique can very accurately find the phase angle at which to measure small changes in capacitance, and can follow the change which occurs in θ over a fivefold increase in the total capacitance. In a similar experiment we have also been able to show that phase tracking can accurately determine θ during a twofold increase in series resistance.

We can also show that with phase tracking methods it is possible to find the change in $|B^2|$ due to cell impedance changes. This is important because the calibration depends linearly on $|B^2|$, and we will use the estimate of the change in $|B^2|$ to update the calibration of the capacitance record. The dashed line in Fig. 2 *D* shows the theoretical dependence of $|B^2|$ on C_m, calculated from Eq. 6. In the simulation, we measured $|\Delta I_{R_s}|$, the current projection at θ-90° for a constant amplitude ΔR_s, after each capacitance increment. Since the value of C_m is known exactly (it is simply C_a), Eq. 5 can be used to find $|B^2|$. The diamonds in Fig. 2 *D* are experimental results. Again, there is close agreement between the theoretical prediction and the measurement (◊) with phase tracking. We should thus be able to use known 1-MΩ series resistance changes to estimate a new calibration for capacitance increases during the degranulation of a real mast cell.

Phase tracking reduces the errors in C_m measurements

Joshi and Fernandez, 1988, derived an expression for the error in estimating the magnitude of a capacitance change measured with a stationary phase detector, due to changes in θ and B^2. This was given by

$$E = 100\left\{1 - \frac{|B^2(t)|\cos[\theta(t) - \theta(0)]}{|B^2(0)|}\right\}, \qquad (12)$$

where $[\theta(t)-\theta(0)]$ is the drift in the phase angle of the capacitance current vector from $t = 0$ to t, due to intervening changes in the cell impedance. $|B^2|$ is as defined in Eq. 6. By keeping the phase detector aligned with ΔI_{Cm}, the phase tracking method eliminates the cosine term from Eq. 12. Thus,

$$E = 100\left[1 - \frac{|B^2(t)|}{|B^2(0)|}\right]. \qquad (13)$$

This remaining error reflects the fact that B^2 also depends on the cell's circuit parameters. However, as described in the calibration section, when using phase tracking we can calculate a factor, *CF*, by which to multiply the measured ΔI_{Cm} that effectively eliminates the errors introduced by the change in $|B^2|$.

Experimental confirmation of Eqs. 12 and 13 and the effect of using *CF* are illustrated in Fig. 3. A model cell (C_m = 2 pF, R_s = 14.7 MΩ) was connected to the input of the patch clamp amplifier as in the experiments of Fig. 2, *C* and *D*. The capacitance circuitry is used to simulate 100-fF capacitance steps and the overall increase in "membrane" capacitance of the model cell. We measured the error in estimating the amplitude of 100-fF C_m steps, due to the increase in capacitance from the initial value (2 pF), according to

$$E = 100\ (1 - \text{size at } C_{new}/\text{size at 2 pF}). \qquad (14)$$

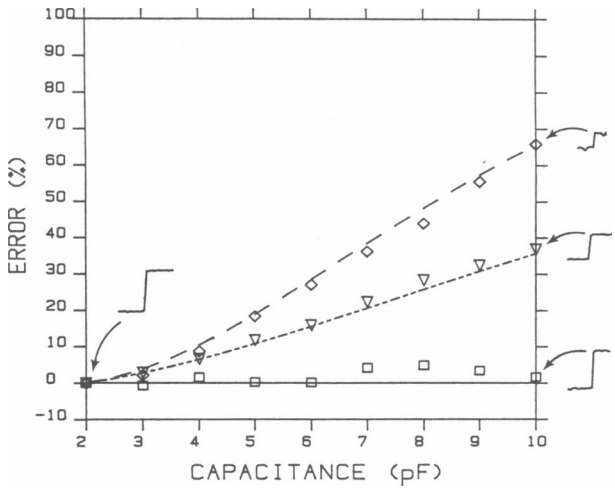

FIGURE 3 Phase tracking eliminates the errors in measuring small changes in capacitance following large increases in C_m. The simulation assumes an initial C_m = 2 pF, R_s = 4.7 MΩ, and ω = 5,234/s. The upper curve (— — —) is the theoretical error calculated from Eq. 12, which is the case for a stationary phase detector (i.e., no phase tracking). Diamonds (◇) are experimentally determined errors, obtained by measuring the reduction in amplitude of a ΔC_m = 100 fF, such as those shown in the insets at 2 and 10 pF. The middle curve (-------) is the error calculated from Eq. 13, and the inverted triangles (▽) are the measured error with phase tracking. Applying an experimentally determined correction, *CF* (see text), to each data point (▽) results in the error plotted as squares (□).

Diamonds in Fig. 3 correspond to the measured error when phase tracking was not used, and the detector remains fixed at the initial angle appropriate only for C_m = 2 pF. Superimposed on the experimental values is the error predicted from Eq. 12 (— — —). An example of the reduction in the apparent size of the 100-fF steps which occurs without phase tracking is shown in the insets at 2 pF and 10 pF next to the upper curve.

If the same experiment is repeated using phase tracking to keep the detector aligned with ΔI_{Cm} following each capacitance increase, then the measured errors decrease significantly (▽, Fig. 3). Again, the experimental results coincide with the predicted error from Eq. 13 (-------). Also, compare the size of a 100-fF step change in C_m with and without phase tracking in the insets at 10 pF.

To correct this remaining error we used the method outlined in the calibration section. In the experiment of Fig. 3 we know exactly the starting and current value of C_m and can measure the magnitude of the projection at θ-90° for a constant amplitude ΔR_s following each C_m increment. From Eq. 11, we determined *CF* and corrected the current changes obtained with phase tracking by this amount. This results in each corrected 100-fF step being equal in amplitude (error free) over the whole capacitance range (□, Fig. 3). Thus, by experimentally determining the change in $|B^2|$ from the current projections due to known R_s changes and correcting the data by this factor, we have essentially eliminated all errors encountered when the cell impedance changes by a large factor.

Experiments with mast cells

We have demonstrated the usefulness of the phase tracking technique in measurements of secretion in GTP-γS stimulated mast cells. A typical experiment is shown in Fig. 4. The top trace in this figure is a low gain record of the capacitance increase. The initial membrane capacitance for this cell was 3 pF and increased to a final value of 10.4 pF. The 1-pF scale bar was determined for the starting cell parameters (initial R_s = 6.3 MΩ), and is only accurate in the early part of the recording when the C_m

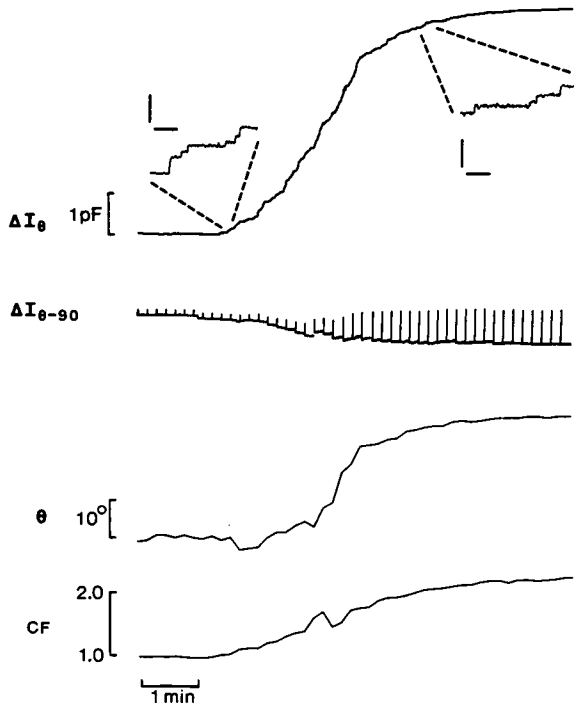

FIGURE 4 Phase tracking applied to measurements of secretion in mouse peritoneal mast cells. The traces labeled ΔI_θ and $\Delta I_{\theta\text{-}90}$ are the currents recorded by two orthogonal outputs of the phase detector. The top trace is recorded at the phase angle θ, and therefore indicates changes in capacitance only. The 1-pF scale bar shown to the left of the trace was determined shortly after breaking into the cell. The scale bars for both enlarged insets are 50 fF and 1 s. The third trace, labeled θ, shows the time course of the phase angle at which the detector is set to measure capacitance. In this experiment, two measurements of ΔI_{R_s} were averaged to calculate the phase angle. The last trace is the time course of *CF*, calculated from Eq. 11, in which $C_m(0)$ is the starting capacitance, 3 pF, and $|\Delta I_{R_s}(0)|$ is the magnitude of the first 1-MΩ current projection shown in $\Delta I_{\theta\text{-}90}$. $C_m(t)$ and $|\Delta I_{R_s}(t)|$ are determined for each subsequent frame.

increase was less than about 30%. This macroscopic C_m increase was recorded at an amplifier gain of 10 mV/pA, and the records can also be examined with this same gain to visualize the individual fusion events, as shown in the two insets at the beginning and end of the degranulation. With one technique we can obtain the overall membrane expansion and the single granule fusion events for an entire degranulation.

Current monitored by the other phase detector output, i.e., at θ-90°, is shown in the second trace of Fig. 4. The contribution to this component due to the typical R_m changes that occur in mast cells is so small that this trace essentially indicates the changes that occurred in R_s only. The regularly spaced current projections in this trace are produced by transiently opening the relay and adding 1 MΩ to the series resistance of the cell. This is done each time a new phase angle is found and immediately after the phase detector outputs are set at θ and θ-90°. Thus, the current displacements also act as a marker each time phase tracking is used. Note that the 1-MΩ change in R_s causes a deflection at θ-90° only, and there is no effect on the ΔI_θ trace, indicating that the correct phase angle is found each time. The sixfold increase in the size of these 1-MΩ current projections is a direct measure of how severely the calibration of the R_s trace is affected by the fourfold increase in C_m. It was for this reason that no scale bar was indicated for the $\Delta I_{\theta\text{-}90}$ trace. Instead, keep in mind that each vertical deflection indicates the magnitude of a 1-MΩ increase in R_s at that instant. Of course, in regions where there is no change in the cell impedance, there is no corresponding change in the size of the 1-MΩ calibrations.

The third trace in Fig. 4 shows the change that occurs in θ as the cell degranulated. Note that the largest rate of change of θ occurred during the steepest increase in capacitance, as expected, and that toward the end of the degranulation where the cell's impedance was fairly constant, θ was also constant. The absolute value of θ is unimportant; only the change in θ is of interest. As seen, θ increased ~32° by the end of the degranulation. Because the series resistance decreased slightly in this experiment, the change in θ was smaller than usual.

The capacitance data is still affected by the change in the proportionality between ΔI_{C_m} and ΔC_m. In Fig. 4, ΔI_θ is not corrected for this change in scale, and so the fusion events detected at the end of the recording appear reduced in amplitude by the same factor as $|B^2|$. Using Eq. 11 we calculated the correction factor, *CF*, by which the C_m steps should be multiplied to obtain the accurate sizes based on the 1-pF calibration at the start of the record. The time course of *CF* is plotted in the lower trace of Fig. 4. *CF* remained ~1 until the cell started to degranulate. At the second inset of steps near the end of the record, *CF* had increased to ~2, indicating that $|B^2|$ and thus the C_m scale have been reduced by one half. This means that the C_m steps in the second inset are half as large as they should appear.

A useful way to judge the impact that changes in $|B^2|$ have on the size of the individual fusion events is to compare a histogram of granule sizes before and after correction by *CF*. This is shown in Fig. 5. The solid line is a histogram of the C_m steps obtained with phase tracking from the raw data, ΔI_θ, in Fig. 4. Each step was then multiplied by the corresponding *CF* to obtain the "true" size distribution histogram (*dashed line*, Fig. 5). We determined the correction for each frame of data and multiplied all of the capacitance steps in the frame by *CF*. From Eq. 11, *CF* was calculated for the *j*th frame from a measure of the 1-MΩ R_s projection in the *j*th frame and in the *O*th frame (in which the initial calibration is found) and from a knowledge of the total capacitance at frames *O* and *j*. We know the initial capacitance, based on the initial cancellation of the cell's capacity transient, and keep a cumulative estimate of the total cell capacitance to find C_m at frame *j*. We have written a simple computer subroutine to implement the correction of all the capacitance steps by the determined amount (*CF*) for all the frames of data. As a result of this correction, it is seen that a shift of ~5 fF occurs in the location of the peak of the histogram. This may be smaller than expected because, even though *CF* gets as large as 2.2, comparatively few

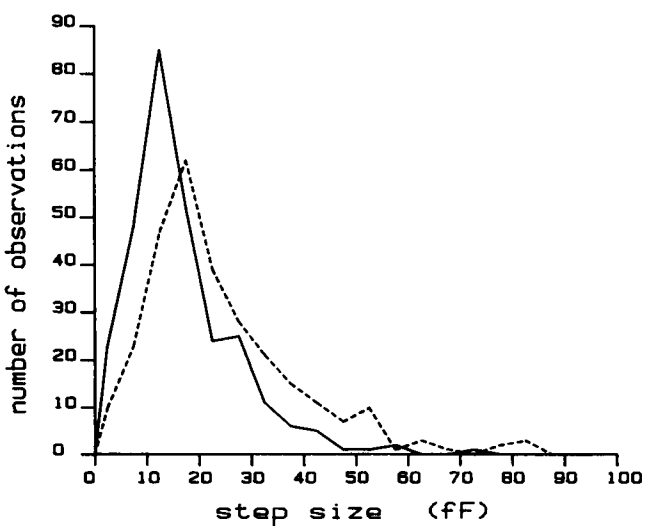

FIGURE 5 Comparison of amplitude histograms of individual fusion events obtained with phase tracking before and after correction for the changes in $|B^2|$. The size, in femtofarads, of nearly all the capacitance increases observed for the cell in Fig. 4 are plotted in the solid line histogram. The total number of observations is 303, the bin width is 5 fF, and the lines connect the center of each bin. The result of applying a correction to the C_m step sizes produces a shift in the histogram to larger values as indicated by the dotted line histogram. The shift in the peak of the histogram is 5 fF.

steps occur near the end of the degranulation as opposed to the middle when CF is only ~1.5. The impact of the correction, however, would be much larger if significant series resistance increases occurred during the recording.

DISCUSSION

Throughout this paper, we have simplified the mathematical analysis by assuming that R_m was large compared with the impedance of C_m, and could thus be ignored. How would a membrane resistance < 500 MΩ, for example, affect measurements of C_m changes with phase tracking? Phase tracking will still enable one detector output to always be aligned perpendicular to R_s changes. However, a low R_m causes the angle between the R_s vector and the C_m vector to be slightly less than 90°. For such cells, the detector would therefore be a few degrees away from the maximum capcitance signal. Because R_s changes are often larger and more unpredictable than R_m changes, it may still be more important to be perpendicular to R_s changes. This must be evaluated for each particular cell system.

The concept of phase tracking can easily be generalized to the use of other circuit components. For instance, if instead of a 1-MΩ resistor in series with the cell, we used a capacitor or inductor, we could obtain current projections at other phase angles. This allows for the design of various strategies that may permit a direct computation of the cell capacitance in real time. We have, in fact, been able to use the two measured quantities from the 1-MΩ R_s changes (the magnitude and phase of ΔI_{Rs}) to solve for the two unknown cell parameters (R_s and C_m), again making the assumption that $R_m \gg 1/\omega C_m$. We were able to calculate the absolute value of C_m in real time with no need for finding θ. However, this method was limited by the resolution of our analog to digital converter and was much less sensitive than the phase detection technique. It should certainly be possible to improve the sensitivity of such a method, and also to include other circuit elements to produce known perturbations of the cell current in order to calculate all three parameters, C_m, R_s, and R_m, in real time.

In this paper we have shown that phase tracking can be used to determine the appropriate phase angle at which to measure current proportional to capacitance changes, both in a model system and in mast cells. As the phase of the capacitance vector moves, phase tracking can rapidly and accurately locate the new phase angle and keep the detector aligned with the capacitance signal. Series resistance changes do not appear in the capacitance output and therefore do not get misinterpreted as capacitance changes. Typical increases in θ for mast cells are as much as 70° and usually occur when the three- to fourfold increase in capacitance is also accompanied by an increase in R_s. Without phase tracking in such cases, the detector output would be so misaligned that step capacitance changes could not be resolved, and in fact would artifactually project on the series resistance output. We have found this to be the most important advantage of phase tracking. It is now possible to routinely record an entire degranulation, and resolve single granule fusion events even at the end of the recording, irrespective of the large changes in any of the cell's electrical parameters. Another important advantage of phase tracking is that the method for determining θ does not depend on the capacitance cancellation circuitry of the amplifier, unlike previous methods for finding θ. The phase angle found with the phase tracking technique depends on the cell's electrical parameters only.

We have also described a method for calculating the change in the calibration scale which occurs whenever there are large changes in the cell input impedance. This method was shown to be accurate for a model cell and eliminated all remaining errors in estimating the size of small capacitance increases. We also applied the correction to mast cells to obtain the "true" size distribution histogram of granule fusion events measured for the degranulation of a single cell. With mast cells, however, there is as yet no way to prove, unambiguously, that we have obtained the exact size distribution. What is needed to confirm such results is a method to estimate accurately the surface areas of all the granules before stimulation and recording with patch-clamp techniques. This could perhaps be achieved using light microscopy and quantitative image processing techniques. Then, a comparison of the corrected amplitude histogram of granule sizes, obtained with phase tracking, with the results obtained with light microscopy should prove to be a reliable test of the ability to correct for the changing calibration scale in real cells. Nevertheless, phase tracking clearly improves the accuracy and extends the time range for measuring capacitance changes due to the fusion of individual secretory granules, and should prove invaluable in quantitating the amplitude and kinetic features of secretion in single cells.

We thank Dr. G. Alvarez de Toledo for comments, discussions, and for his separate evaluation of the use of phase tracking with mast cells. We also thank Dr. R. J. Bookman, Dr. D. E. Clapham, and Chaya Joshi for valuable suggestions on the manuscript.

The research reported here was supported by National Institutes of Health grant GM-38857.

Received for publication 13 April 1989 and in final form 27 July 1989

REFERENCES

Breckenridge, L. J., and W. Almers. 1987*a*. Final steps in exocytosis observed in a cell with giant secretory granules. *Proc. Natl. Acad. Sci. USA*. 84:1945–1949.

Breckenridge, L. J., and W. Almers. 1987*b*. Currents through the fusion pore that forms during exocytosis. *Nature* (*Lond.*). 328:814–817.

Cole, K. S. 1935. Electric impedance of Hipponoe eggs. *J. Gen. Physiol.* 18:877–887.

Fernandez, J. M., E. Neher, and B. D. Gomperts. 1984. Capacitance measurements reveal stepwise fusion events in degranulating mast cells. *Nature* (*Lond.*). 312:453–455.

Fidler, N., and J. M. Fernandez. 1989. Phase tracking: a new technique for cell membrane capacitance measurements. *Biophys. J.* 55:599*a*. (Abstr.)

Gillespie, J. I. 1979. The effect of repetitive stimulation on the passive electrical properties of the presynaptic terminal of the squid giant synapse. *J. Physiol.* (*Lond.*). 206:293–306.

Hamill, O. P., A. Marty, E. Neher, B. Sakmann, and F. J. Sigworth. 1981. Improved patch-clamp techniques for high-resolution current recording from cells and cell-free membrane patches. *Pfluegers Arch. Eur. J. Physiol.* 391:85–100.

Jaffe, L. A., S. Hagiwara, and R. T. Kado. 1978. The time course of cortical vesicle fusion in sea urchin eggs observed as membrane capacitance changes. *Dev. Biol.* 67:243–248.

Joshi, C., and J. M. Fernandez. 1988. Capacitance measurements: an analysis of the phase detector technique used to study exocytosis and endocytosis. *Biophys. J.* 53:885–892.

Lindau, M., and J. M. Fernandez. 1986. IgE-mediated degranulation of mast cells does not require opening of ion channels. *Nature* (*Lond.*). 319:150–153.

Lindau, M., and E. Neher. 1988. Patch-clamp techniques for time-resolved capacitance measurements in single cells. *Pfluegers Arch. Eur. J. Physiol.* 411:137–146.

Mason, W. T., S. K. Sikdar, R. Zorec, S. Akerman, S. R. Rawlings, T. Cheek, R. Moreton, and M. Berridge. 1989. Ion channels, intracellular calcium, and exocytosis: control of hormone secretion in cultured bovine pituitary lactotrophs. *In* Secretion and Its Control. The Rockefeller University Press, New York. 44:225–238.

Neher, E. 1988. The influence of intracellular calcium concentration on degranulation of dialysed mast cells from rat peritoneum. *J. Physiol.* (*Lond.*). 395:193–214.

Neher, E., and A. Marty. 1982. Discrete changes of cell membrane capacitance observed under conditions of enhanced secretion in bovine adrenal chromaffin cells. *Proc. Natl. Acad. Sci. USA*. 79:6712–6716.

Schweizer, F. E., T. Shafer, C. Tapparelli, M. Grob, U. O. Karli, R. Heumann, H. Thoenen, R. J. Bookman, and M. M. Burger. 1989. Inhibition of exocytosis by intracellularly applied antibodies against a chromaffin granule-binding protein. *Nature* (*Lond.*). 339:709–712.

Zimmerberg, J., M. Curran, F. S. Cohen, and M. Brodwick. 1987. Simultaneous electrical and optical measurements show that membrane fusion precedes secretory granule swelling during exocytosis of beige mouse mast cells. *Proc. Natl. Acad. Sci. USA*. 84:1585–1589.